AIMS Bioengineering

AIMS Bioengineering, 9(3): 1–7.
DOI: 10.3934/bioeng.2022017
Received: 17 June 2022
Revised: 11 August 2022
Accepted: 26 August 2022
Published: 30 August 2022

http://www.aimspress.com/journal/Bioengineering

Research article

Signal transduction from ligand-receptor binding associated with the formation of invadopodia in an invasive cancer cell

Noorehan Yaacob[1,*], Sharidan Shafie[1], Takashi Suzuki[2] and Mohd Ariff Admon[1]

[1] Department of Mathematical Sciences, Faculty of Science, Universiti Teknologi Malaysia, Skudai, 81310 Johor Bahru, Johor, Malaysia
[2] Center for Mathematical Modeling and Data Science, Osaka University, Japan

* **Correspondence:** Email: noorehanyaacob@gmail.com.

Abstract: Invadopodia are finger-like protrusions that are commonly spotted at the membrane of the invasive cancer cell. These structures are a major cause of death among cancer patients through metastasis process. Signal transduction stimulated upon contact between ligand and membrane receptors is identified as one of key factors in invadopodia formation. In this study, a time-dependent mathematical model of signal and ligand is investigated numerically. The moving boundary of plasma membrane is taken as a zero-level set function and is moved by the velocity that accounted as the difference of gradient between intra-cellular signal and extra-cellular ligand. The model is solved using a combination of ghost with linear extrapolation and finite difference methods. The results showed that the stimulation of signal from membrane associated ligand consequently moved the plasma membrane outward as time increases. The highest densities of signal and ligand are recorded on the membrane and slowly diffused into intra-cellular and extra-cellular regions, respectively.

Keywords: ghost fluid method; invadopodia; level set method; ligand; protrusion; signal transduction

Appendix: The numerical scheme

The equations in Section 2.1 are numerically solved using the second order centered finite difference and ghost fluid with linear extrapolation for the discretization of regular and neighboring points, respectively. The regular point is the point that is distant from the interface and the neighboring point is the point that is close by the interface. The existence of regular and neighboring points is shown in Figure 6. Apart from that, the movement of the free boundary interface is detected by the zero-level set function. In this paper, the number of lattice points along x and y axes are taken as (M_x, M_y).

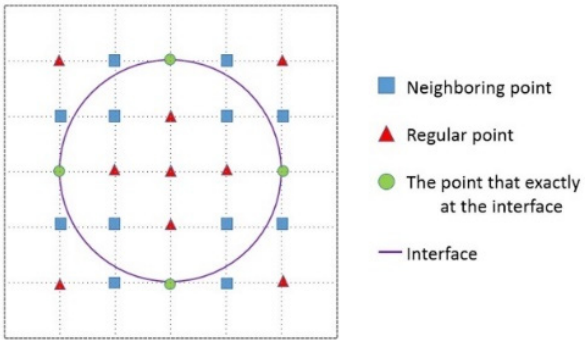

Figure 6. The existence of points on the grid.

A.1 Initial Level Set Function

The study on the level set method is focused mostly on tracking the shape or boundary changes. The exploration of the level set method is first introduced by [22] to capture the moving fronts in many multi-physics problems. A review on the level set techniques to many problems is stated in [23]. Further study on the level set method has been done by [24] which highlighted the Stefan problem. Stefan problem is related to the evolution of smooth boundaries for different phases in a pure substance, for instance, the changes from solid ice to water. Other exploration on the level set method is conducted by the studies in [25–27]. They proposed the numerical scheme for the level set method which combines with the front-tracking and fixed domain methods to model the growth and interaction of multiple dendrites in solidification.

In this paper, the level set method is employed to detect the motion of the interface. The regions of intra-cellular and extra-cellular can also be determined using this method. Firstly, the level set function, $\psi_{i,j}$ is set as the equation of a circle. The circle obtained is to portray the individual invasive cancer cell. From the equation of circle, the regions of the interface, intra-cellular, and extra-cellular are observed by using the approach of $\psi_{i,j}^t = 0, \psi_{i,j}^t < 0$, and $\psi_{i,j}^t > 0$, respectively. Afterward, the discretization for the Laplace operator in ligand and signal is solved.

A.2 Numerical Discretization

In this section, the discretization technique is presented. The forward finite difference as in Eq 5 is used for the discretization of time. There are two different methods applied for the discretization of the Laplace operator in ligand and signal. At the regular point, the second order centered finite

difference is implemented for the x and y axes as in Eqs 6,7, respectively. Suppose $u_{i,j}^n$ is the signal and ligand densities at the position of (i,j) and time n.

$$(u_t)_{i,j} = \frac{u_{i,j}^{n+1} - u_{i,j}^n}{k}, \tag{5}$$

where k denoted timestep.

$$(u_{xx})_{i,j}^n = \frac{u_{i+1,j}^n - 2u_{i,j}^n + u_{i-1,j}^n}{h^2}, \tag{6}$$

$$\left(u_{yy}\right)_{i,j}^n = \frac{u_{i,j+1}^n - 2u_{i,j}^n + u_{i,j-1}^n}{h^2}, \tag{7}$$

where h is the step length for x and y axes.

The second order centered finite difference is not appropriate to apply for the neighboring point because for this approach, five-point stencil is needed. However, for the neighboring point, one of the neighbors is on the other side of the interface. This point is named the ghost point and will be linearly extrapolated. Hence, the ghost fluid method with linear extrapolation is suitable to apply. Equations in (8), (9), (10), and (11) are the discretization for the neighboring points from four different directions. These equations are only focused on the intra-cellular or signal region. Let $u_{i,j}^n$ is the signal concentration at the position of (i,j) and time n.

Left neighboring point:

$$(u_{xx})_{i,j}^n = \frac{2}{(1+\theta_x)h^2} u_{i+1,j}^n - \frac{2}{\theta_x h^2} u_{i,j}^n + \frac{2}{\theta_x(1+\theta_x)h^2} u_\Gamma^n. \tag{8}$$

Right neighboring point:

$$(u_{xx})_{i,j}^n = \frac{2}{(1+\theta_x)h^2} u_{i-1,j}^n - \frac{2}{\theta_x h^2} u_{i,j}^n + \frac{2}{\theta_x(1+\theta_x)h^2} u_\Gamma^n. \tag{9}$$

Below neighboring point:

$$\left(u_{yy}\right)_{i,j}^n = \frac{2}{\left(1+\theta_y\right)h^2} u_{i,j+1}^n - \frac{2}{\theta_y h^2} u_{i,j}^n + \frac{2}{\theta_y\left(1+\theta_y\right)h^2} u_\Gamma^n. \tag{10}$$

Above neighboring point:

$$\left(u_{yy}\right)_{i,j}^n = \frac{2}{\left(1+\theta_y\right)h^2} u_{i,j-1}^n - \frac{2}{\theta_y h^2} u_{i,j}^n + \frac{2}{\theta_y\left(1+\theta_y\right)h^2} u_\Gamma^n. \tag{11}$$

As shown in the above equations, the θ_x and θ_y are clarified as the distance of points x_i and y_j to the interface, respectively. Suppose θ_x or θ_y is equal to one, hence the points are situated exactly on the grid. Thus, the θ_x and θ_y are determined as in Eq 12,13, respectively.

$$(\theta_x)_{i,j}^n = \begin{cases} \dfrac{\psi_{i,j}^n}{\psi_{i,j}^n - \psi_{i-1,j}^n}, & x \in \left[x_{i-1,j}, x_{i,j}\right], \\ -\dfrac{\psi_{i,j}^n}{\psi_{i+1,j}^n - \psi_{i,j}^n}, & x \in \left[x_{i,j}, x_{i+1,j}\right]. \end{cases} \tag{12}$$

$$(\theta_y)_{i,j}^n = \begin{cases} \dfrac{\psi_{i,j}^n}{\psi_{i,j}^n - \psi_{i,j-1}^n}, & y \in [y_{i,j-1}, y_{i,j}], \\ -\dfrac{\psi_{i,j}^n}{\psi_{i,j+1}^n - \psi_{i,j}^n}, & y \in [y_{i,j}, y_{i,j+1}]. \end{cases} \tag{13}$$

In some cases, there are possibilities to have the interface located in between horizontal meshes (left and right), vertical meshes (below and above), and both meshes. Assume that there is an occurrence of a neighboring point from the left side as in Figure 7 and as shown in the figure, there are two points separated by the interface. One of the points is on the regions of intra-cellular (signal) and the other point is on the extra-cellular (ligand) region. Hence Eq 14 is implemented for the point in intra-cellular region while Eq 15 is applied for the point in extra-cellular region.

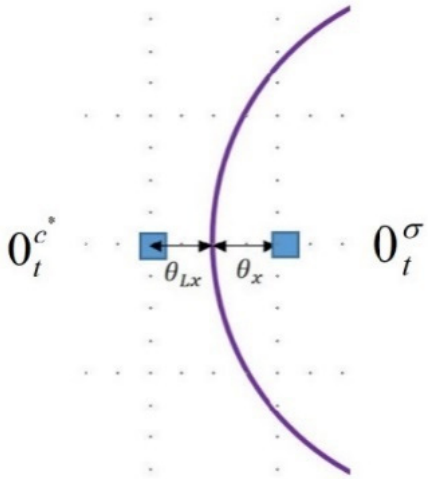

Figure 7. Interface located in between two horizontal meshes with left θ_x to the neighboring point.

$$u_{i,j}^{n+1} = u_{i,j}^n + \frac{k}{h^2}\left[\frac{2}{(1+\theta_x)}u_{i+1,j}^n - \left(\frac{2}{\theta_x}+2\right)u_{i,j}^n + \frac{2}{\theta_x(1+\theta_x)h^2}u_{\Gamma_x}^n + u_{i,j+1}^n + u_{i,j-1}^n\right]. \tag{14}$$

$$u_{i,j}^{n+1} = u_{i,j}^n + \frac{k}{h^2}\left[\frac{2}{(1+\theta_{Lx})}u_{i-1,j}^n - \left(\frac{2}{\theta_{Lx}}+2\right)u_{i,j}^n + \frac{2}{\theta_{Lx}(1+\theta_{Lx})h^2}u_{\Gamma_x}^n + u_{i,j+1}^n + u_{i,j-1}^n\right]. \tag{15}$$

In addition, there is also a situation where the interface is located in between two meshes as in Figure 8. At this point, two neighboring points are spotted, which are left and below sides from the interface. In this case, Eq 16 is employed.

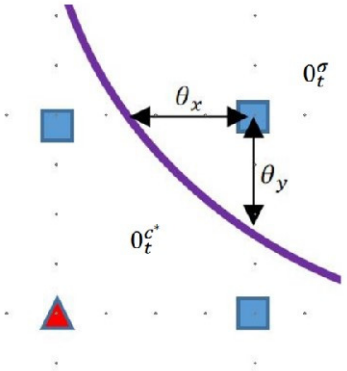

Figure 8. Interface located in between four meshes with left θ_x and below θ_y to the neighboring point.

$$u_{i,j}^{n+1} = u_{i,j}^{n} + \frac{k}{h^2}\left[\frac{2}{(1+\theta_x)}u_{i+1,j}^{n} + \frac{2}{(1+\theta_y)}u_{i,j+1}^{n} - \left(\frac{2}{\theta_x}+\frac{2}{\theta_y}\right)u_{i,j}^{n} + \frac{2}{\theta_x(1+\theta_x)h^2}u_{\Gamma_x}^{n} + \frac{2}{\theta_y(1+y)h^2}u_{\Gamma_y}^{n}\right]. \tag{16}$$

A.3 Velocity on the Interface

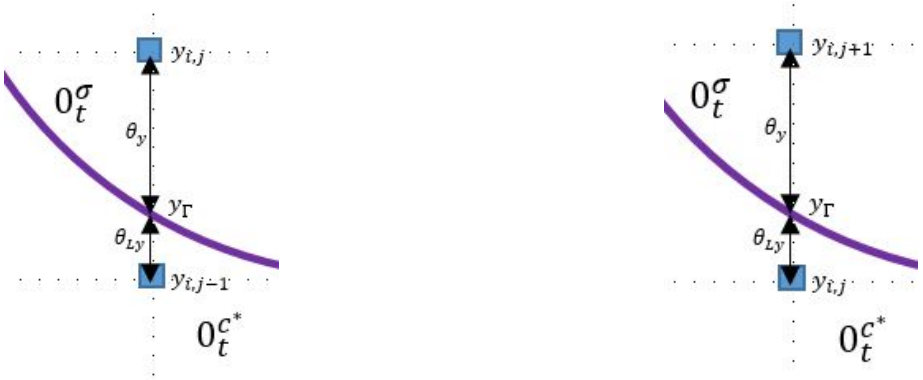

(a) (b)

Figure 9. The velocity on the interface for the regions of (a) signal and (b) ligand.

The polymerization of actin led to the movement of the interface. In the meantime, the interface is detected by using the method of the level set where the interface is appointed to the zero-level set function. Study in [16,17] accounted for the polymerization of actin as the gradient of the intra-cellular signal. In this paper, the mathematical modeling for actin is predicted as the difference of gradient between intra-cellular signal and extra-cellular ligand. Figure 9a,b represented the velocity on the interface for signal and ligand regions, respectively. In the figures, the velocity on the y axis is brought into focus. Eqs 17,18 are the technique used to obtain the velocity information on both signal and ligand positions, respectively.

Velocity on the interface for signal region:

$$v_y^n = \frac{\sigma_{i,j}^n - \sigma_\Gamma^n}{\theta_y h} - \frac{{c^*}_\Gamma^n - {c^*}_{i,j-1}^n}{\theta_{Ly} h}. \tag{17}$$

Velocity on the interface for ligand region:

$$v_y^n = \frac{\sigma_{i,j+1}^n - \sigma_\Gamma^n}{\theta_y h} - \frac{{c^*}_\Gamma^n - {c^*}_{i,j}^n}{\theta_{Ly} h}. \tag{18}$$

A.4 Velocity Extensions

$$(\psi_x)_{i,j}^n = \begin{cases} \dfrac{\psi_{i,j}^n - \psi_{i-1,j}^n}{h}, & \text{for } \partial\Omega_x^+, \\ \dfrac{\psi_{i+1,j}^n - \psi_{i,j}^n}{h}, & \text{for } \partial\Omega_x^- \\ \dfrac{\psi_{i+1,j}^n - \psi_{i-1,j}^n}{2h}, & \text{otherwise.} \end{cases} \tag{19}$$

$$(w_x)_{i,j}^n = \begin{cases} \dfrac{w_{i,j}^n - w_{i-1,j}^n}{h}, & \text{if } \psi_x > 0, \\ \dfrac{w_{i+1,j}^n - w_{i,j}^n}{h}, & \text{if } \psi_x < 0, \end{cases} \tag{20}$$

where $\partial\Omega_x^-$ and $\partial\Omega_x^+$ are left and right boundaries, respectively.

In numerical computation, the velocity extension is crucial to prevent discontinuities on the interface. In many studies, the velocity is mentioned only on the interface. However, dealing with the level set method, the details of velocity on the interface with the whole domain is required. Hence, the velocity needs to be extended to recapture the velocity on each area from the interface. The study on the velocity extension has been widely explored in [28] and in this paper, the method of fast marching is applied for treating the velocity extension. On the other hand, in this paper, the velocity extension is calculated using Eq 4. Directing to the x axis, this equation is discretized using Eqs 19,20 where Eq 20 is based on upwind technique.

A.5 Update the Level Set Function

The level set method is used to detect the movement of the free boundary interface by setting the interface as the zero-level set function. After receiving the velocity information on each area from the interface, the level set function needs to be updated by utilizing the equation of transport. In this case, the gradient of ψ is formulated to the second-order upwind approach (see Eq 21) instead of the first-order upwind scheme. As mentioned by [16], to get better volume conservation, second-order upwind is more appropriate to deal with since it is less dispersive compared to the first-order upwind method. On that account, the level set function is updated using the Eq 22.

$$(\psi_x)_{i,j}^n = \begin{cases} \dfrac{-\psi_{i+2,j}^n + 4\psi_{i+1,j}^n - 3\psi_{i,j}^n}{2h}, & \text{if } (v_x) < 0, \\ \dfrac{3\psi_{i,j}^n - 4\psi_{i-1,j}^n + \psi_{i-2,j}^n}{2h}, & \text{if } (v_x) > 0, \\ 0, & \text{if } (v_x) = 0, \end{cases}$$

$$(\psi_y)_{i,j}^n = \begin{cases} \dfrac{-\psi_{i,j+2}^n + 4\psi_{i,j+1}^n - 3\psi_{i,j}^n}{2h}, & \text{if } (v_y) < 0, \\ \dfrac{3\psi_{i,j}^n - 4\psi_{i,j-1}^n + \psi_{i,j-2}^n}{2h}, & \text{if } (v_y) > 0, \\ 0, & \text{if } (v_y) = 0. \end{cases} \tag{21}$$

$$\psi_{i,j}^{n+1} = \psi_{i,j}^n - \Delta t\left[\left((v_x)_{i,j}^n\right)\left((\psi_x)_{i,j}^n\right) + \left((v_y)_{i,j}^n\right)\left((\psi_y)_{i,j}^n\right)\right]. \tag{22}$$

Note that, $(v_x)_{i,j}^n = (w_x)_{i,j}^n$ and $(v_y)_{i,j}^n = (w_y)_{i,j}^n$, on the interface.